# Characterization of Supersonic Laboratory-Scale Jet Noise with Vector Acoustic Intensity

Kent L. Gee[1]
*Brigham Young University, Provo, UT, 84602*

Masahito Akamine[2] and Koji Okamoto[3]
*The University of Tokyo, Kashiwa, Chiba, 277-8561, Japan*

Tracianne B. Neilsen[4] and Mylan R. Cook[5]
*Brigham Young University, Provo, UT, 84602*

Seiji Tsutsumi[6]
*Japan Aerospace Exploration Agency, Sagamihara, Kanagawa, 252-5210, Japan*

*and*

Susumu Teramoto[7] and Takeo Okunuki[8]
*The University of Tokyo, Bunkyo, Tokyo, 113-8656, Japan*

**A new method for the calculation of vector acoustic intensity from pressure microphone measurements has been applied to the aeroacoustic source characterization of an unheated, Mach 1.8 laboratory-scale jet. Because of the ability to unwrap the phase of the transfer functions between microphone pairs in the measurement of a radiating, broadband source, physically meaningful near-field intensity vectors are calculated up to the maximum analysis frequency of 32 kHz. The new intensity method is used to obtain a detailed description of the sound energy flow near the jet. The resulting intensity vectors have been used with a ray-tracing technique to identify the dominant source region over a broad range of frequencies. Additional aeroacoustics analyses provide insight into the frequency-dependent characteristics of jet noise radiation, including the nature of the hydrodynamic field and the transition between the principal lobe and sideline radiation.**

## Nomenclature

$d$ = spacing between two microphones
$D_j$ = nozzle exit diameter
$H_{a,b}$ = transfer function between microphones $a$ and $b$
$\mathbf{I}$ = time-averaged vector intensity
$p$ = acoustic pressure
$P$ = acoustic pressure magnitude
$\phi$ = acoustic pressure phase
$Q_{a,b}(\omega)$ = quadspectrum between microphones $a$ and $b$

---

[1] Associate Professor, Dept. of Physics and Astronomy, N283 ESC, AIAA Senior Member.
[2] Ph.D. Candidate, Dept. of Advanced Energy, Graduate School of Frontier Sciences, AIAA Member.
[3] Associate Professor, Dept. of Advanced Energy, Graduate School of Frontier Sciences, AIAA Member.
[4] Part-Time Assistant Professor, Dept. of Physics and Astronomy, N283 ESC, AIAA Member.
[5] M.S. Candidate, Dept. of Physics and Astronomy, N283 ESC.
[6] Associate Senior Researcher, Aerospace Research and Development Directorate, Research Unit III, AIAA Member.
[7] Senior Engineer, Dept. of Aeronautics and Astronautics, Graduate School of Engineering.
[8] Associate Professor, Dept. of Aeronautics and Astronautics, Graduate School of Engineering, AIAA Senior Member.

American Institute of Aeronautics and Astronautics

$r$     =   position vector
$\rho_0$     =   ambient density of air
St     =   Strouhal number
$t$     =   time
$u$     =   acoustic particle velocity
$x$     =   axial distance
$\mathbf{X}$     =   microphone position difference matrix
$z$     =   sideline (radial) distance

## I.  Introduction

CHARACTERIZATION of the aeroacoustic noise source region in turbulent jets using acoustical measurements is most often carried out using directional microphone arrays. Directionality in response may be achieved through an elliptic mirror[1] or through digitally steering received signals in a beamforming algorithm[2,3]. Although beamforming is a convenient approach, traditional beamforming processing algorithms usually assume mutual source incoherence, which can lead to errors when the source has finite correlation lengths. This is particularly true for the large-scale features of a jet. Cross-beamforming methods[4] that seek an inverse solution to the measured field, similar to near-field acoustical holography[5,67], can account for the partial coherence, but are still subject to the same bandwidth limitations due to array aperture and interelement spacing.

This paper describes the use of vector acoustic intensity to directly characterize the time-averaged energy flow near a supersonic, laboratory-scale jet. Despite acoustic intensity's use as robust engineering tool to obtain sound power[8,9,10], identify sources[11] and characterize building transmission properties[12], the measurement technique has not been heavily utilized to characterize the source region of turbulent jet flows. One possible reason for this is that the active acoustic intensity, which is the time-averaged product of pressure and particle velocity, describes the sound power flux at a single location, and it takes a set of these measurements to characterize the radiated field.  Another possible reason is the relatively limited bandwidth of the traditional cross-spectral intensity method, due to microphone phase mismatch at low frequencies and theoretical bias errors and intensity probe scattering at high frequencies.

Until recently, the use of intensity in aeroacoustics source and field characterization was relatively sparse. Ventakesh et al.[13] briefly described the use of a one-dimensional intensity probe to validate the results of a new beamforming algorithm for distributed, broadband sources. Yu et al.[14] developed a surface-normal intensity inverse method to characterize source regions, with specific application to aeroacoustics. The most extensive use of the technique, however, rests with Jaeger and Allen,[15] who performed bandlimited, two-dimensional vector intensity measurements of a laboratory-scale, unheated jet with Mach numbers ranging from 0.2 to 0.6. For each jet condition, the authors determined the intensity angle as a function of frequency then traced intensity vectors directly back to the jet centerline, using the intercepts to describe the source region. As expected from the low Mach numbers, the intensity vectors were found to originate from a relatively compact region downstream of the nozzle, with the source location traveling upstream as a function of frequency.   Importantly, they showed that intensity measurements made at a sideline distance of 4.5 $D_j$ predicted the source region to be upstream of those predicted by the polar correlation method of Fisher et al.[16], although at a sideline measurement distance of 20 $D_j$, the two methods better agreed. They attributed the disagreement at 4.5 $D_j$ to "near-field distortion" of the intensity measurement.

This paper describes the application of the recently developed phase and amplitude gradient estimator (PAGE) method[17,18] for calculating vector acoustic intensity to the wideband near-field characterization of a laboratory-scale supersonic jet. The present study builds upon the original Jaeger and Allen study of unheated jets and more recent efforts to characterize full-scale rocket plume[19,20,21] and military jet engine[22,23] noise environments.  The      intensity method is first summarized, followed by a description of the experimental facilities and measurement performed. The traditional and PAGE methods are compared in their abilities to obtain physically reasonable results, and the PAGE method is used to characterize the jet noise source. Properties of the hydrodynamic near field are also examined. In addition to physical insights regarding this supersonic, unheated jet, the analyses results point to the potential of vector intensity to improve characterization of supersonic jet noise sources and near-fields.

## II.  Acoustic Intensity and the PAGE Method

The time-averaged vector acoustic intensity stems from the product of the time-dependent pressure and vector particle velocity,

American Institute of Aeronautics and Astronautics

$$I = \frac{1}{T} \int p(t)\boldsymbol{u}(t)dt, \tag{1}$$

where the bold-faced notation indicates a vector. From two well matched microphones, Fahy[24] and Pavic[25] determined a means to calculate the frequency-domain intensity spectrum, still the standardized approach used today. The time-averaged acoustic intensity component along the $x$ axis for two microphones spaced $d$ apart is written as

$$I_x(\omega) = \frac{1}{\rho_0 \omega d} Q_{2,1}(\omega), \tag{2}$$

where $\rho_0$ is the ambient density and $Q_{2,1}(\omega)$ is the quadspectrum (the imaginary part of the cross spectrum) between the two microphones. From the single-axis intensity probes, many have developed multidimensional acoustic intensity probes. For these probes involving multiple combinations of microphone pairs, the optimal intensity calculations are obtained using least-squares weighting of quadspectra, as described by Pascal and Li[26] and Wiederhold *et al.*[27,28] The bias errors associated with the traditional method have generally resulted in substantial bandwidth limitations. For example, intensity magnitude errors for two well-matched microphones separated by 25 mm in a propagating plane wave field exceed 1 dB beginning at about 2.5 kHz. For many laboratory-scale applications, this is at or below the peak frequency region of the spectrum in the dominant radiation direction.

The PAGE method[17] improves on the traditional cross-spectral approach by estimating gradients of the pressure phase and amplitude across a multimicrophone probe to calculate the complex intensity. The complex intensity is comprised of two parts – the active and reactive portions. The active intensity describes the radiated acoustic field that stems from the product of the pressure and the in-phase component of particle velocity. On the other hand, the reactive component describes the amplitude of the oscillations for which pressure and particle velocity are in quadrature. The methodology builds from the work of Mann[29,30,31] and colleagues, who theoretically interpreted the radiated intensity and other energy-based quantities. As part of their work, they expressed the spatially dependent complex pressure at position, $\boldsymbol{r}$, in terms of a pressure magnitude and phase, $p(\boldsymbol{r}) = P(\boldsymbol{r})e^{-j\phi(\boldsymbol{r})}$. By Euler's equation for a time-harmonic acoustic process, the particle velocity is calculated in terms of $\nabla p$ as

$$\boldsymbol{u}(\boldsymbol{r}) = \frac{j}{\rho_0 \omega} \nabla p = \frac{1}{\rho_0 \omega} [P(\boldsymbol{r})\nabla\phi(\boldsymbol{r}) + j\nabla P(\boldsymbol{r})]e^{-j\phi(r)}, \tag{3}$$

which, from Eq. (1), results in an expression for the radiated (active) intensity as

$$I = \frac{1}{2\rho_0 \omega} P^2 \nabla\phi = \frac{1}{\rho_0 \omega} \overline{P^2}\nabla\phi, \tag{4}$$

where $\overline{P^2}$ is the mean-square pressure. Although Mann *et al.*[29] onsidered this alternate expression theoretically, it is noteworthy that Mann and Tichy[31] stepped from this expression directly to the traditional cross-spectral approach when describing actual measurements.

In the PAGE method, $\overline{P^2}$ can be readily found by locating a microphone at the acoustic center of the probe or, alternatively, by finding a least-squares estimate of the pressure magnitude[26,27]. (For the probe geometry used in the experiments, a microphone was located at the probe center.) The phase gradient, $\nabla\phi$, is calculated for $N$ microphones located at positions, $\boldsymbol{r_{1..N}}$, by first defining a position difference matrix, $\boldsymbol{X}$, written as

$$\mathbf{X} = [\boldsymbol{r_2} - \boldsymbol{r_1}| \dots |\boldsymbol{r_N} - \boldsymbol{r_{N-1}}]^T \tag{5}$$

and then finding the least-squares estimate for the gradient, expressed as

3
American Institute of Aeronautics and Astronautics

$$\nabla\phi \approx (\mathbf{X}^T\mathbf{X})^{-1}\mathbf{X}^T\Delta\boldsymbol{\phi}. \qquad (6)$$

The ensemble-averaged phase difference between microphones, $\Delta\boldsymbol{\phi}$, in Eq. (4) can be found through the argument of the transfer function between different microphone pairs, written as

$$\Delta\boldsymbol{\phi} = -\left[\arg\{H_{1,2}\}, \ldots, \arg\{H_{N-1,N}\}\right]^T. \qquad (7)$$

Note that whereas the traditional cross-spectral method is limited to well below the spatial Nyquist limit because of the calculation bias errors, the use of the transfer function phase in the PAGE method allows for the direct possibility of phase unwrapping for a broadband source. Initial application of the PAGE method to a plane-wave tube experiment and this datset in Ref. 18 shows the ability to unwrap phase multiple times and extend the frequency bandwidth of the PAGE method more than an order of magnitude beyond the traditional high-frequency limit.

## III. Experiment

### A. Jet Experiment

The experiment was carried out using a jet facility at the Hypersonic High-enthalpy Wind Tunnel at Kashiwa Campus of the University of Tokyo. Although the facility is not anechoic, nearby reflecting surfaces were wrapped in fiberglass. Favorable matches to anechoic measurements by Greska[32] were shown previously by Akamine *et al.* [33] but some multipath interference effects are noted in the measured spectra at the intensity probes, particularly for the measurements made closest to the nozzle. For each jet blow, the jet facility ambient pressure, temperature, and humidity were recorded using a Kestrel 4500B weather station. The average ambient sound speed during the measurements was 348 m/s.

The unheated, Mach-1.81 jet with Re = 6.58e6 was ideally expanded through a 20-mm diameter converging-diverging nozzle, with an the average exit centerline velocity of $U_j = 488$ m/s and a jet sound speed of $c_j = 270$ m/s. The jet "characteristic frequency" $(U_j/D_j)$, which is used to obtain a frequency-to-Strouhal number scaling, is 24.44e3 kHz. Although the jet's Mach number and acoustic Mach number $(U_j/c_\infty =1.40)$ are both supersonic, it is important from a radiation perspective to note this unheated jet's convective Mach number is only weakly convectively supersonic. When typical values of the turbulence convection speed of $0.7 - 0.8$ are used, the jet's convective Mach number ranges between 0.981 and 1.12. These empirical values bound the Oertel-Patz[34,35] definition of the convective Mach number, which yields 1.01, indicating Mach waves have just fully developed.[36] Direct visualization of this jet by Panda *et al.*[37] and Akamine *et al.*[33] using Schlieren reported evidence for Mach wave formation. The Mach number suggests this experiment serves as a convenient transition between convectively subsonic jets and more efficiently radiating supersonic jets.

Other useful properties of the jet that impacts sound radiation are the potential and supersonic core lengths. Baars[36] has helpfully provided a recent review of different formulations for these lengths. Measurements of the centerline velocity by Akamine *et al.*[33] and determination of the end of the constant velocity region suggest a potential core length of ~9 $D_j$, which agrees well with the length determined by Panda and Seasholtz[37] and the 9.1 $D_j$ predicted by the empirical formula of Nagamatsu and Horvay[38]. Based on a similar empirical formula by the same authors, the supersonic core length for this jet is predicted to be 15.3 $D_j$. Note that the Witze[39] model, which is used to collapse centerline velocity decay across different jet conditions (e.g. see Ref. 40), predicts a potential core length of 12.3 $D_j$ and a sonic length of 23.8 $D_j$, both of which are appreciably downstream of the Nagamatsu-Horvay model results and also downstream of the measurements by Panda and Seaholtz and Akamine *et al.*

### B. Acoustical Measurements

Data from two microphone arrays are shown in this paper; both are shown in Fig. 1. First, G.R.A.S. 40BE Type 1 prepolarized microphones were used to create a 16-channel polar microphone arc with 5° resolution spanning 15 – 90°, with angles measured relative to the jet exhaust centerline. The microphones were located at a radial distance of 40 nozzle diameters ($D_j$) and centered 10 $D_j$ downstream from the jet exit. The 10 $D_j$ origin was selected in an attempt to locate the array origin near the maximum radiation location averaged over frequency. Prior elliptic mirror analyses by Viswanathan[41] on an unheated Mach 1.9 jet, flow-acoustics correlation measurements by Panda *et al.*[42], and

American Institute of Aeronautics and Astronautics

beamforming analyses by Lee and Bridges[43] on heated, subsonic jets with similar acoustic Mach numbers were used to guide this selection, but it was recognized at the outset that some low frequencies were likely to originate from regions downstream of 10 $D_j$ and some high frequencies upstream of that location. But, the selection of an appropriate origin that is close to the dominant noise source, as opposed to the nozzle, reduces misalignment between observation radials and direction of propagation, particularly at low frequencies where the source is extended and located appreciably downstream of the nozzle[44,45].

The near-field array consisted of four two-dimensional intensity probes comprised of G.R.A.S. 46BG microphones, which have sensitivities less than 0.3 mV/Pa and permit peak sound pressure level measurements in excess of 180 dB. As shown in Fig. 1, the microphones were arranged in an equilateral triangle by 3D-printed holders, with a microphone at the center of the triangle such that the distance between the center and the vertices was 25.4 mm. Gridcaps were removed for all microphones, both at the arc and the polar array. The four probes were arranged in a linear array, with an interprobe separation distance of 8 $D_j$. For most measurements, the array axis was oriented to be parallel to the shear layer, but was rotated to be perpendicular to the jet centerline for some measurements in order to increase the vertical array aperture along the sideline near the nozzle. This was required because of the limited range-of-travel of the automated 2D stepper motor-driven positioning system used to move the probe array. All the probe measurement positions are shown in Fig. 1. Specific downstream distances ($x = 10.0, 20.0, 24.0, 28.0$, and 29.9) are highlighted with different colors that are used subsequently in analyzing some intensity probe results for ease of distinguishing location. During jet operation, calibrated acoustic pressure waveform data were synchronously acquired at each array position at 204.8 kHz using National Instruments PXI-4498 cards. During each jet blow, which lasted between 60-90 seconds, data were acquired for ~6.1 seconds before moving the array. With an analysis block size of 2048 samples and 50% overlap, this results in approximately 1200 averages per position.
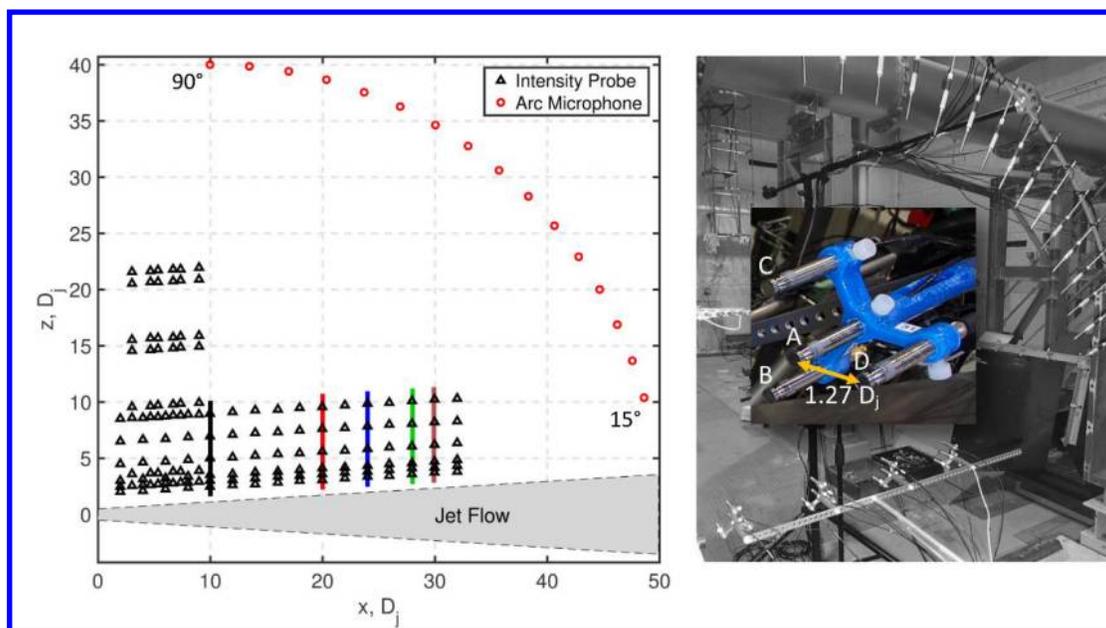


**Figure 1. Left: Locations of the 40 $D_j$ polar microphone array and intensity probe measurement locations. Specific downstream distances are color-coded. Right: A four-microphone, two-dimensional intensity probe, with the microphones labeled A-D. Microphones B-D were parallel to the shear layer for most measurements. Also shown were four probes in a linear array and polar arc. The jet nozzle is located at the lower-left corner of the picture.**

## C. Level-based Results at 40 $D_j$

Some level-based results at the 40 $D_j$ arc are instructive in describing the jet noise radiation features and in demonstrating the need for the PAGE method in determining this laboratory-scale jet's broadband source and near-field characteristics using vector intensity. The power spectral density (PSD) from 0.8 – 50 kHz (St = 0.0328 – 2.05) and overall sound pressure level (OASPL) at the arc are shown in Fig. 2. First, the OASPL is a maximum between 30 – 35° relative to the jet exhaust centerline, which is characteristic of a slightly convectively supersonic jet. Second,

American Institute of Aeronautics and Astronautics

the spectral shape evolves with angle in keeping with the two-source[46] similarity spectra; recent analyses have described large and fine-scale similarity spectra decompositions[47] and modeling for source wavepacket eduction[48] for this jet. Third, the PSD peak frequency shifts between ~2 kHz (St = 0.082) at 15° to 5 – 6 kHz at 65°, beyond which the peak remains relatively constant. Given the relatively high peak frequency, one of the key points of Fig. 2 is the significant limitation of the traditional cross-spectral method in obtaining a broadband aeroacoustic source characterization with the intensity probe geometry. Calculation bias errors limit the vector intensity field with the traditional method to below about 3 kHz (St ≈ 0.12), as prior analyses[49] of this probe configuration suggests magnitude errors exceed 1 dB at 2.5 kHz and directional errors begin to grow rapidly at approximately 5 kHz. Thus, the broadband, vector acoustic intensity field must be obtained using an alternate processing method.
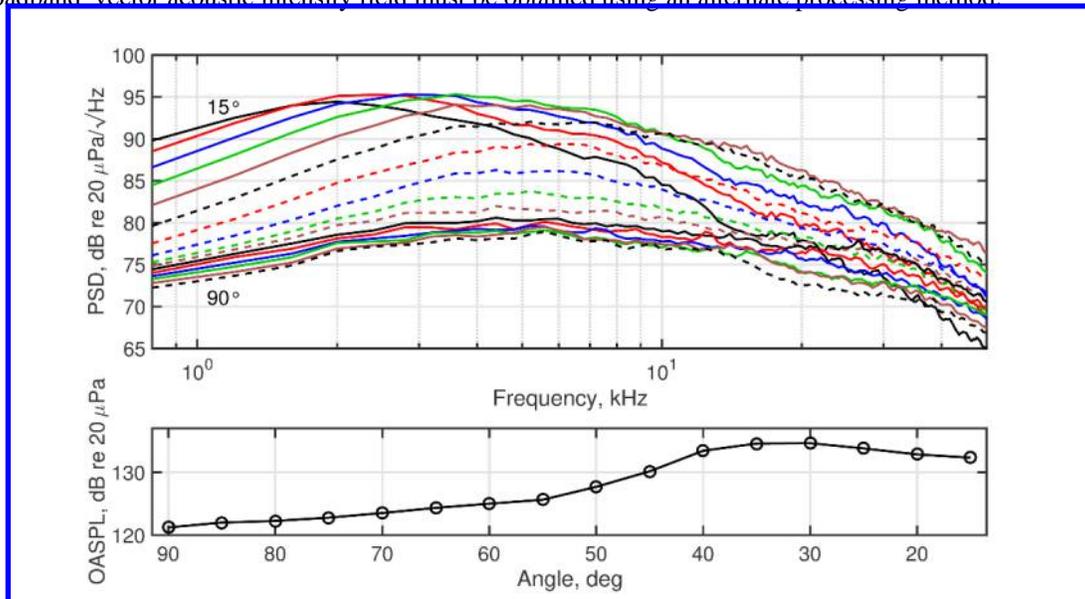


**Figure 2. Power spectral densities and overall sound pressure levels at the microphone arc located at a radial distance of 40 $D_j$ and centered 10 $D_j$ downstream of the nozzle exit.**

## IV. Intensity Analysis

In this section, two analyses demonstrate the utility of the PAGE method. First, the ability to phase-unwrap the transfer functions between probe microphones is demonstrated. This is essential for the use of PAGE above the spatial Nyquist frequency, where otherwise estimates of $\nabla\phi$ would be aliased and highly erroneous. Seconds, comparisons between the traditional and PAGE spectra at a few specific locations are shown to identify the bandwidth limitations of the traditional method in this experiment and further illustrate the promise of the PAGE method in broadband jet aeroacoustic source characterization.

### A. PAGE Phase Unwrapping

As described in Sec. II, the PAGE method formulation allows for the possibility to unwrap the phase of the transfer function and increase the intensity calculation bandwidth. Bandwidth extension is impossible with the traditional method because it employs directly weighted sums of complex cross spectra, which causes significant bias errors as the spatial Nyquist frequency is approached.[17] Figure 3 shows four representative examples of the negative argument of the transfer function between microphones, $\Delta\phi$ in Eq. (7), across intensity probes at different locations in the noise field. Note that the color of the location label corresponds to the marked lines in Fig. 1, whereas the color of the lines are consistent between microphone pairs. Two of the locations are close to the shear layer, with the location at (10.0, 2.49) $D_j$ being near the transition point between sideline and downstream radiation and the other, at (24.0, 3.34) $D_j$ exhibiting downstream behavior. The other two locations, at (24.0,7.60) $D_j$ and (29.9,10.2) $D_j$ are farther from the shear layer. In each plot in Fig. 3, there are six curves, representing the wrapped (dashed lines) and unwrapped (solid lines) frequency-dependent $\Delta\phi$ for the three outer microphones on an intensity probe (see Fig. 1) relative to one another. These pairs are shown because they ultimately are the contributors to the two-dimensional intensity calculation for this probe configuration.[17,49] The results show clearly why, for the sound field radiated by a jet plume, the PAGE method is a viable alternative to the decades-old method of calculating intensity from the complex cross

6

American Institute of Aeronautics and Astronautics

spectra of multimicrophone probes. For $x = 20.0$ and $29.9\ D_j$, the unwrapping occurs between one and five times for the three transfer functions considered, and the unwrapped phase continues smoothly out to the maximum analysis bandwidth of 40 kHz. For $(24.0, 3.34)\ D_j$, the unwrapping occurs between one and five times for the three transfer functions, and though not especially smooth particularly for the microphone pair closest to the shear layer (B:D), the overall phase trend follows a relatively linear form. Examination of the coherence between the three microphone pairs reveals lower coherence for the B:D pair, thus leading to more uncertainty in the $\Delta\phi$ estimate, particularly above 30 kHz. For the most upstream location shown in Fig. 3, $(10, 2.49)\ D_j$, the phase unwraps smoothly to approximately 20 kHz for the B:C and B:D pairs, whereas for C:D, the phase is nearly zero. (The nearly zero phase indicates the dominant wavefronts are traveling perpendicular to the C:D pair axis.) Beyond 20 kHz, the coherence drops markedly for all three microphone pairs, resulting in a non-smooth phase. Poor coherence sometimes leads to phase unwrapping errors and spurious discontinuities, such as those present for $(10, 2.49)\ D_j$ in Fig. 3. A coherence-based phase unwrapping method developed for this analysis helps resolve the majority of phase unwrapping errors caused by the rudimentary MATLAB® "unwrap" function, provided that the phase can be assumed to vary smoothly (appropriate for a jet mixing noise field) and drops in coherence are localized to a limited frequency region. However, in a few locations, like those relatively close to the nozzle or along the lower-amplitude sideline, unwrapping errors persist. These errors describe the anomalous directions of a few of the intensity vectors in Sec. V.

It is important to note that the microphone separation used to obtain broadband intensity is relatively large; microphone separations of 25–50 mm have been used previously for full-scale military jet engines[22,23] and even larger-scale solid rocket motor tests[19,20,21]. The ability to extract time-averaged phase relationships and produce intensity vectors in the near field from microphones that are ultimately multiple wavelengths apart is unique and shows the utility of phase unwrapping for extending probe bandwidth well beyond traditional limits for broadband sources.
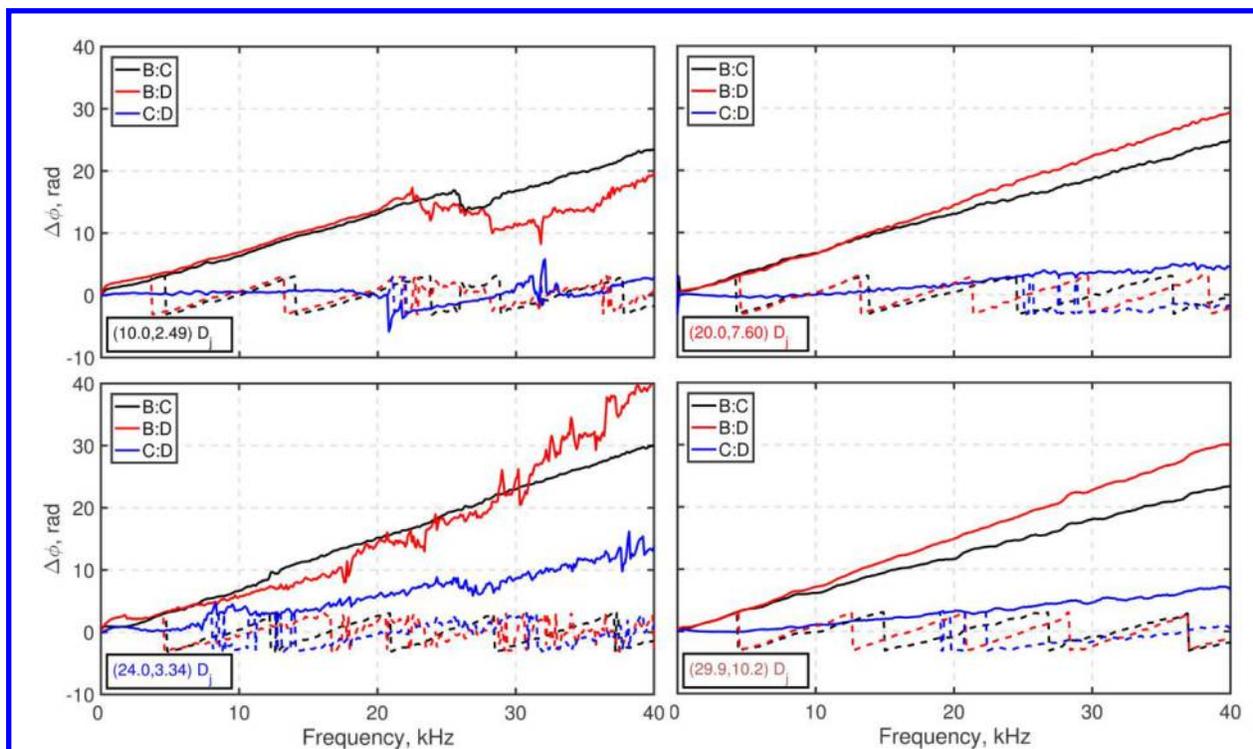


**Figure 3. Unwrapped transfer function for the outer three microphone pairs using coherence-based unwrapping at locations along four downstream distances shown in Fig. 1. Irregular regions coincide with poor coherence.**

## B. Intensity Spectra Comparison

Analytical investigations with simple sources[17,50] and measurements with loudspeakers in planar[18] and free-field propagation environments[49] have shown the significant improvement that the PAGE method provides over the

American Institute of Aeronautics and Astronautics

traditional method bias errors. An initial study[18] of intensity bandwidth extension by phase unwrapping was recently conducted to show its feasibility for laboratory-scale jet noise, but is considered here in more detail.

Intensity magnitude spectra shown for the same locations as in Fig. 3 help to illustrate the PAGE intensity calculation process around a jet. Because the active intensity field is obtained from the portion of the particle velocity that is in phase with the pressure, for any propagating acoustic wave field, $|I| \propto \overline{P^2}$, and the sound pressure and intensity levels are equivalent to with 0.2 dB. (The difference is due to rounding in the standardized decibel reference for sound pressure level). This near equivalence becomes a convenient benchmark for the PAGE-based intensity magnitudes.

The intensity levels calculated with both the traditional ($L_I^{TRAD}$) and PAGE ($L_I^{PAGE}$) methods, along with the sound pressure levels ($L_p$) at microphone A, are displayed in Fig. 4 for the same four probe locations in Fig. 3. Because of the calculation bias errors, $L_I^{TRAD}$ errors exceed 1 dB between 3-4 kHz. For these locations, the PAGE intensity levels closely approximate the sound pressure levels, to within 0.5 dB, at most frequencies. At $(10.0, 2.49)$ $D_j$, it is apparent that the phase unwrapping errors above 20 kHz in Fig. 3 have only a marginal effect (<2 dB) on $L_I^{PAGE}$, but serves as an important reminder that the $\nabla\phi$ estimate impacts both the intensity direction *and* magnitude. Overall, the concordance of $L_I^{PAGE}$ with $L_p$ illustrates the validity of the phase unwrapping at high frequencies in most cases. At $(10.0, 2.49)$ $D_j$ and $(24.0, 3.34)$ $D_j$, both $L_I^{TRAD}$ and $L_I^{PAGE}$ are greater than the pressure level at low frequencies (less than ~3 kHz). Proximity to the shear layer and substantially elevated low-frequency levels in the case of $(24.0, 3.34)$ $D_j$ (the spectral peak is at about 500 Hz or St = 0.020 ) suggest a likely influence of the hydrodynamic pressure field on the intensity level. Location of intensity probes within the hydrodynamic near field is further considered as part of the PAGE near-field intensity characterization in Secs. V and VI.
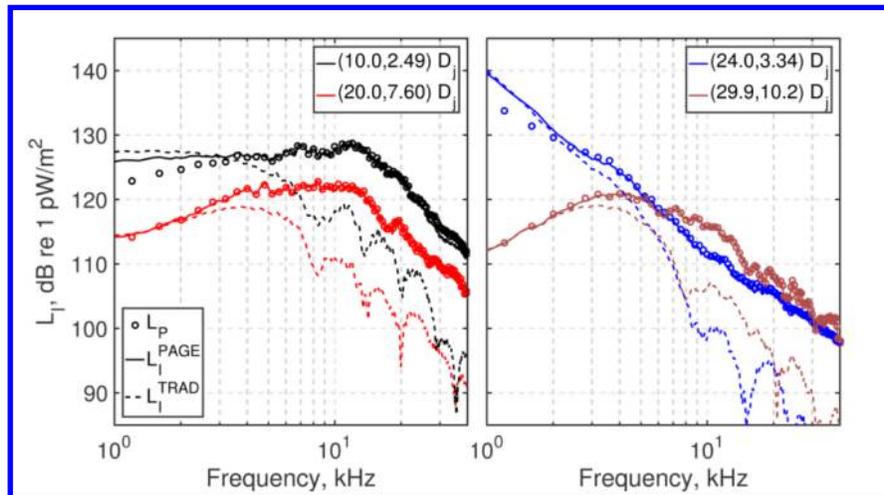


**Figure 4. Intensity spectra levels, along with the sound pressure level, at the four locations shown in Fig. 4 near the Mach 1.8, unheated jet. Line colors correspond to the various downstream lines shown in Fig. 1.**

## V. PAGE Method Near-field Intensity Characterization

### A. Intensity Mapping

The success of the phase unwrapping method and agreement of intensity and sound pressure levels suggest that the PAGE method, which has been previously used with various probe geometries to produce full-scale rocket and military jet noise source characterizations from as low as 30 Hz to as high as 6 kHz, can be extended to much higher frequencies for this experiment. While less important for a full-scale rocket motor with dominant radiated intensity below 100 Hz[19,21], the frequencies in the several kilohertz range are critical to the characterization of this small-scale jet. Figure 5 displays narrowband intensity vector and level-based maps for this unheated, Mach 1.8 jet at eight one-third octave band center frequencies from 1.0 kHz to 40 kHz. These frequencies correspond to a Strouhal number range of 0.041 to 1.64, which spans the radiated peak-frequency region in all directions from 15° to 90° (see Fig. 2). In Fig. 5, the jet shear layer is denoted by the dashed line, and vectors appear at all measurement locations shown previously in Fig. 1. For ease in viewing the vector field, the vector lengths have been scaled by the eighth-root of the intensity magnitude. In the intensity level map, color gradations represent 1 dB changes in level. To help provide

American Institute of Aeronautics and Astronautics

physical level estimates in the regions where there are not vector measurements, the sound pressure levels at 40 $D_j$, which, again, should be essentially equal to the intensity levels, are included in the calculation of the interpolated levels.

The PAGE method, combined with phase unwrapping, produce intensity maps that appear physical over the entire analysis bandwidth. First, the angle of the principal radiation lobe increases with frequency, while the sideline radiation appears to be more consistent. Second, the source region that produces this lobe significantly contracts and shifts upstream for much of the frequency range. Before discussing these statements more quantitatively, however, some additional comments regarding Fig. 5 are merited.

Additional features in Fig. 5 are noteworthy. First, at 1.0 kHz and to some extent, 2.0 kHz, the intensity probe locations closest to the jet can be described as being in the hydrodynamic field because the vectors are directly parallel to the jet shear layer. (This phenomenon is also evident with the traditional processing method, i.e., it is not an artifact of the PAGE processing method.) At 1.0 kHz (St = 0.041), these closest vectors dominate the intensity level and demonstrate the propagation behavior of the low-frequency spectral increases in pressure traditionally associated with the hydrodynamic field. At 2 kHz, the vectors closest to the shear layer are again parallel to the jet boundary downstream of ~20 $D_j$. The hydrodynamic field phenomenon is further discussed in Sec. VI. The maps between 4.0 and 8.0 kHz (St = 0.16 and 0.33), which serve to characterize the peak-frequency region of the spectra around the maximum radiation direction, reveal a unidirectionality of the intensity vectors that points to an extended Mach wave source region, with a significant contraction of length in source region between the two frequencies. Futhermore, at these frequencies, there is a sharp transition in radiation characteristics between the downstream Mach wave radiation and the sideline radiation. This sharp transition was also observed in high-speed Schlieren imaging[51] of the same jet and compared to preliminary intensity calculations. Beginning with around 16.0 kHz (St = 0.66), there is a less well-defined transition between the radiation in these two directions. Furthermore, the sideline radiation becomes relatively greater in amplitude. Based on the physical consistency of the vector magnitudes and directions, which are well correlated with the 40 $D_j$ frequency-dependent pressure levels, the PAGE method with phase unwrapping extends the upper useable frequency of the multimicrophone probe hardware to at least 40 kHz, where the number of anomalously pointed vectors seems to appreciably grow.
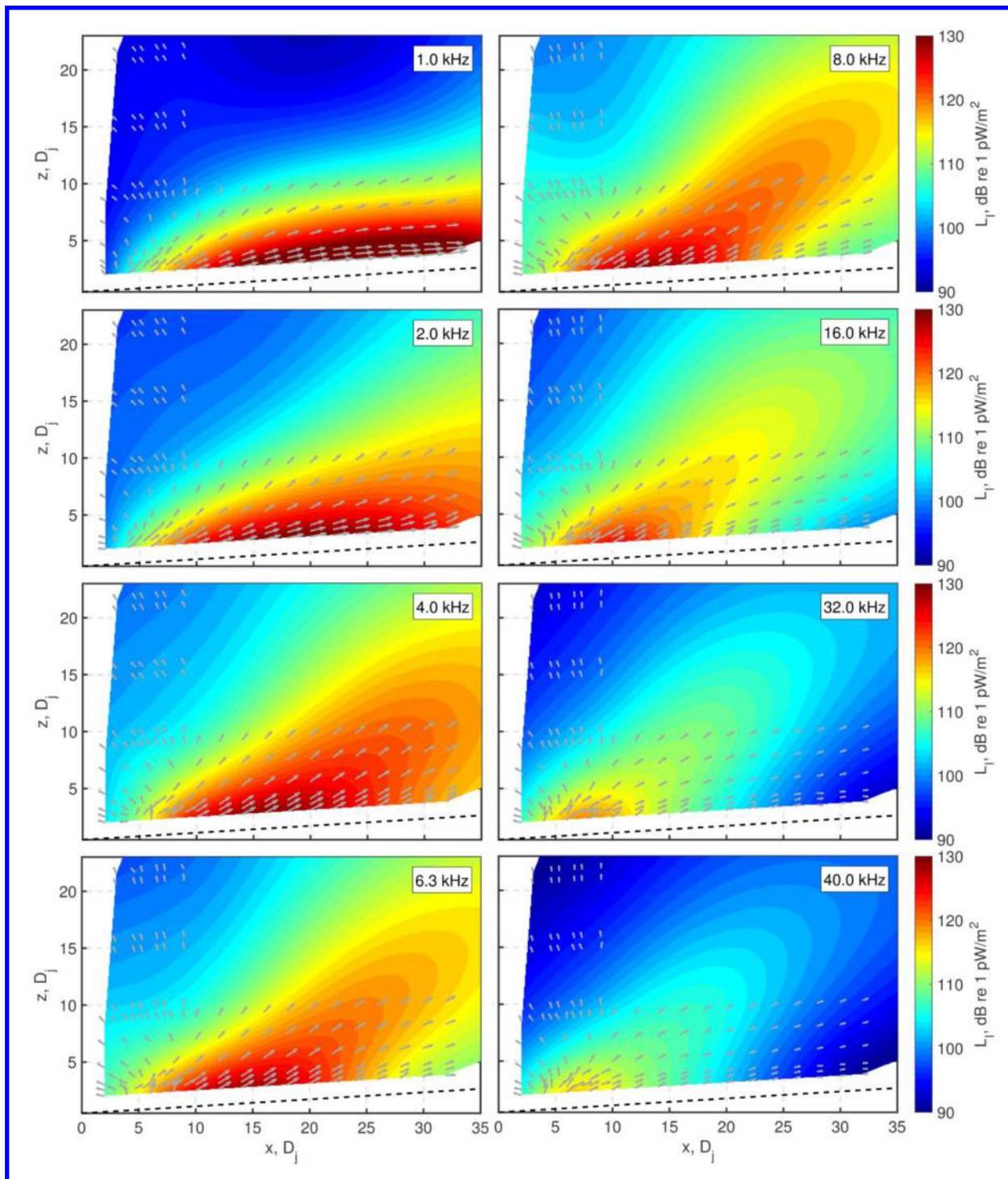
American Institute of Aeronautics and Astronautics

**Figure 5. PAGE-calculated intensity vectors at four frequencies for a Mach 1.8, uheated jet.**

## B. Intensity Angle

Prior intensity analyses of full-scale military jets[23] and rocket motors[20,21] have examined the directional behavior of a linear array of intensity vectors to examine agreement with far-field directivity. A similar analysis, conducted here with a relatively dense intensity array measurement and high-resolution polar arc, provides an important

10

American Institute of Aeronautics and Astronautics

connection to those full-scale measurements. For these measurements, the line of probe locations spanning $z = 6.5$ to 8.4 $D_j$ has been used for this purpose because its offset from the shear layer is similar to the prior full-scale analyses and is largely outside the hydrodynamic field for most frequencies. To obtain the maximum intensity angular range, an interpolation of intensity magnitude and direction was first performed to find the intensity magnitudes within 3 dB of the maximum amplitude vector along this line. Then, minimum and maximum angles for the intensity vectors within this 3-dB region were found. The resulting angular span is shown in Fig. 6 as a function of frequency.

The near-field intensity vector directions in Fig. 6 agree fairly well with the 40 $D_j$ maximum directivity in Fig. 2, both in terms of OASPL and for a broad range of frequencies. The OASPL in Fig. 2 peaks between 30°-35°, and the near-field peak intensity angle averages approximately 32° between 2-10 kHz. The shift to shallow radiation angles at lower frequencies (the maximum levels at 40 $D_j$ occur at ≤15° below 1.6 kHz) is largely captured by the near-field intensity angle, but it is recognized based on the intensity maps in Fig. 5 that 40 $D_j$ is unlikely to be in the far field at low frequencies and there is likely a misalignment between predominant propagation direction from an extended source and observation radials defined at a point. A similar discussion of misalignment of propagation direction and observation radials can also be had about high frequencies, although for this case the source region is relatively compact. Above 16 kHz (St = 0.66) in Fig. 5, the dominant source location appears to be upstream of the $x = 10$ $D_j$ origin of the polar arc, which can also skew the measured spectral levels in a frequency-dependent fashion and explains the discrepancy between the dominant intensity angles between 10-15 kHz being shallower than the 40 $D_j$ PSD would suggest. As an example, at 15 kHz, the 40 $D_j$ PSD suggest a peak directivity around 35°. However, the dominant intensity angle is somewhat less, centered around ~31°. Above about 20 kHz (St = 0.82), Fig. 6 shows a broadening of the intensity angle, something also seen by Stout et al.[23] for F-22 measurements. This is likely due to a merging of the dominant intensity lobe with the sideline radiation, although admittedly some of the noisiness of the angular span is due to likely phase unwrapping errors in the low-amplitude, sideline region.
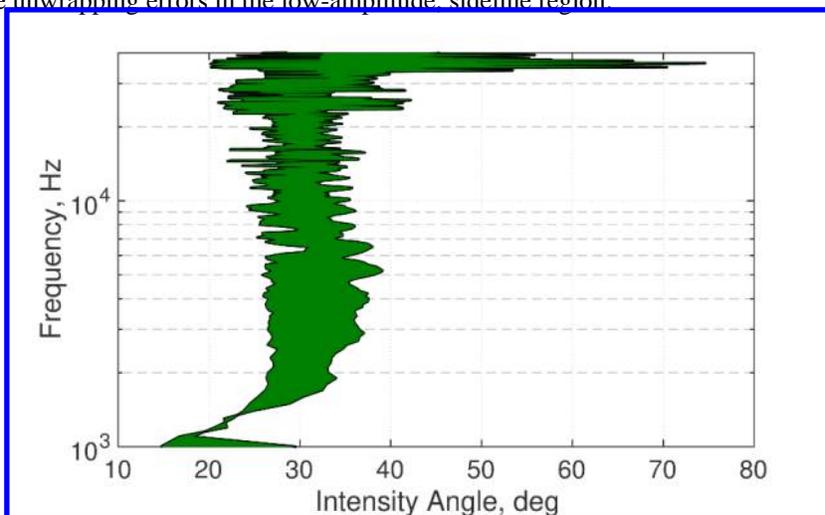


**Figure 6.  Measured intensity angle span within the 3-dB down region of the maximum amplitude intensity vector at the probe locations spanning $z = 6.5$ to 8.4 $D_j$.**

## C.  Maximum Source Raytracing

These intensity measurements have the potential to lend physical insight to source characteristics beyond prior far-field phased-array studies that have attempted to identify noise source distributions as a function of angle. In conjunction with the intensity angle analysis, a similar 3-dB down raytracing analysis was performed. Stout et al.[23] found that using a 3-dB down threshold in the field for raytracing resulted in the ~1-dB-down source region being identified. Again, linear interpolation between measurement points between $z = 6.5$ to 8.4 $D_j$ is used to determine the location of points at which the sound intensity is within 3 dB of the maximum intensity along the measurement line and the intensity vectors within this region are traced back to the jet centerline. The farthest upstream and downstream intercepts of the raytraced vectors along the centerline are used to define the maximum source region. Tracing to the shear layer, as opposed to the centerline, is also a possibility, but the centerline is used for a few reasons. First, it is consistent with the approach of Jaeger and Allen[15], although it should be noted that the authors simply traced all measured vectors without consideration of amplitude. Second, it is the same method employed with recent military

11
American Institute of Aeronautics and Astronautics

jet and rocket noise investigations[21,22,23], so the approach establishes a connection with full-scale studies. Third, although the current approach neglects jet refraction effects, identification of source locations along the centerline is justified by prior work on a Mach 1.8 unheated jet by Panda $et$ $al.$[37,42] that shows that the maximum correlation between the jet's turbulent fluctuations and the far-field acoustic pressure was along the centerline, downstream of the potential core. Raytracing to the centerline suggests that the possible downstream bounds of the maximum source region at the jet centerline is being established.

The 3-dB down raytracing results for the Mach 1.8 unheated jet are shown in Fig. 7 from 1.0 – 40.0 kHz (St = 0.041 – 1.64). From 3.0 – 30.0 kHz (St = 0.12 − 1.23), the raytraced maximum source region contracts from $x = 8.5$ - 15.2 $D_j$ to 0.9 - 2.1 $D_j$. The frequencies that contribute most to the PSD in the 30°-35° maximum OASPL direction are approximately 3 – 7 kHz (St = 0.123 – 0.287), which is consistent with supersonic jet noise understanding[52]. It is significant that the extent of the raytraced source at 3.0 kHz spans nearly exactly the locations between the potential and supersonic core tips, which, as noted previously, occur at 9.1 and 15.3 $D_j$ according to the Nagamatsu and Horvay[38] model. This strengthens work[38] that suggests the dominant noise generation occurs between the two core tips. At around 7 kHz, the dominant raytraced noise source occurs between 6 – 10 $D_j$, which would put it near the end of the potential core. The continued movement of the traced noise source upstream to $x = $ ~1.5 $D_j$ by 30 kHz suggests the importance of the sources near the shear layer, given the ideal expansion of the jet and the location of the potential core collapse. The importance of high-frequency shear layer sources that are correlated with radiation in the maximum direction has been studied by Panda $et$ $al.$[42] and Papamoschou $et$ $al.$[53]

The behavior below 3 kHz and above 30 kHz in Fig. 7 is tied to the low and high-frequency phenomena already mentioned – the hydrodynamic field influence and the blurring between the sideline and downstream radiation phenomena. Below 3 kHz, the vector angles shift toward the shear layer in Fig. 5 as the offset in $z$ is decreased. This causes the ray-traced source region to shift far upstream to clearly nonphysical locations. With this raytracing method, a vector that points directly along the shear layer because of the hydrodynamic field influence would intercept the centerline significantly upstream of the nozzle. Although this invalidates the raytracing method, the turning point at around 2 -3 kHz helps to define the frequency and spatial region at which the hydrodynamic field amplitude begins to become an appreciable fraction of the acoustic field's amplitude. This point is further discussed in Sec. VI. At frequencies greater than 30 kHz, the blending of the downstream radiation, which originates increasingly closer to the nozzle, and sideline radiation produces a 3-dB region that, when ray-traced, broadens. The upstream radiation now falls within the 3-dB down region and accounts for the suddenly larger downstream centerline intercept, while the portion of the 3-dB down region that radiates in the downstream direction results in the relatively smooth variation in the upstream extent of the dominant source region. Thus, this raytracing yields the dominant equivalent centerline source location between 3.0 – 30.0 kHz (St = 0.12 – 1.23), with additional physical insights regarding the source characteristics above and below that frequency range.

It is important to note that other source localization criteria or methodologies are possible, and other localization techniques may result in different source interpretations. Consequently, comparison of this raytraced intensity source region with other source localizations of laboratory-scale jets is informative. First, Panda $et$ $al.$[42] showed that the noise measured at 30° and 50 $D_j$ was most correlated with the turbulent density and density-squared velocity fluctuations along the centerline at around 12 $D_j$. That is in remarkably good agreement with the ray-traced intensity results in Fig. 7 for the peak frequencies present in the 30° PSD in Fig. 2, despite the neglect of any refraction effects. Second, the elliptic mirror measurements of Viswanathan[41] for a Mach 1.9 unheated jet show the peak overall noise distribution for his inlet angle of 150° is centered between ~8 - 17 $D_j$. Third, Papamoschou $et$ $al.$'s[53] beamforming analysis of a Mach 1.75, unheated jet indicated that the maximum noise distribution moved upstream from ~15 $D_J$ to 3 $D_j$ from St = 0.1 to 1.0. A comparison of Fig. 7 with their Fig. 7 indicates that the intensity analysis suggests a greater shift of the maximum noise source region upstream. This greater shift is actually in keeping with their Fig. 17, which showed that the maximum correlation between the nozzle lipline-beamformed acoustical measurements and turbulence measurements occurred at ~2 $D_j$ for St > 0.6. Thus, the intensity measurements provide a stronger connection between the turbulence and the far-field acoustic radiation than just far-field analysis alone. It further indicates that the high-frequency, downstream noise does, in fact, originate from the shear layer upstream of the potential core, rather than from the centerline.

One final comparison of Fig. 7 is with linear sideline beamforming measurements by Lee and Bridges[43] on heated, subsonic jets of similar acoustic Mach number, ranging from 1.32 to 1.47. The results for maximum source location as a function of frequency (see their Figs. 17 and 18) indicate similar locations for high frequencies (St > 0.4), but the locations of the lower frequency noise in the case of the unheated supersonic jet here appear to be substantially downstream than those beamformed by Lee and Bridges. The sudden change in slope of their beamformed source trends around St = 0.4 could be an important distinction between subsonic and supersonic jets, but further

12

American Institute of Aeronautics and Astronautics

investigation is required. Overall, however, the comparisons between other source eduction methods and the raytraced intensity results in this paper help confirm the validity of the PAGE method with phase unwrapping, which then provides additional insights about the energy flow around a Mach 1.8 unheated jet.
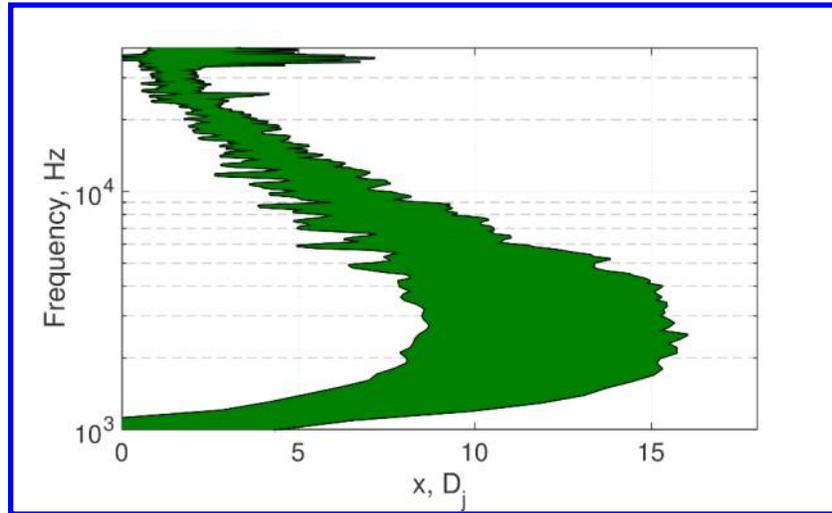


**Figure 7. Apparent source region extent at the Mach 1.8 unheated jet centerline as a function of frequency as ray-traced from the probe locations within 3 dB of the maximum intensity level between z = 6.5 and 8.4 D<sub>j</sub>.**

## VI.   Hydrodynamic Near-field Analysis

The near-shear layer intensity spectra in Fig. 5 and the spatial maps in Fig. 6 indicate that the hydrodynamic near field plays a role in the total measured intensity. The joint presence of the hydrodynamic and acoustic fields has recently been reviewed and investigated by Grizzi *et al*. (see Ref. 54 and references therein) and Kuo *et al.* (see Ref. 55 and references therein.) Both studies employed different means to try to separate the two contributors to near-field pressure fluctuations. No attempt to separate the hydrodynamic fluctuations from the acoustic fluctuations is performed here. Instead, some observations regarding its properties are made, based on the present measurements.

First, is a confirmation that the intensity results at 1.0 kHz in Fig. 5 are heavily influenced by the hydrodynamic field. One way this has been done in the past has been to examine the radial decay of squared pressure, which should be exponential (because of its evanescent, non-radiating nature) rather than follow $1/r$ in the case of cylindrical spreading or $1/r^2$ for spherical spreading.  The intensity decay of a purely supersonic, extended source should transition from near cylindrical spreading in the near field to spherical spreading to the far field.  Figure 8 shows the radial decay of $L_I^{PAGE}$ along the five lines previously noted in Fig. 1.  At 1.0 kHz, for which the hydrodynamic field contribution appears to be strongest in Fig. 5, the intensity decay along all five lines is much faster than $1/r^2$, and as expected, the slope begins to lessen as $z$ increases and the radiated field becomes more prevelant.  At 2.0 kHz, the overall decay is closer to the inverse square law, and at 4.0 kHz the intensity level decreases and increases as the measurement lines slice through the directional radiation lobe.  Note that this analysis is not entirely conclusive by itself in a quantitative sense, as the jet noise at each frequency may be described as comprised of multiple modes, some of which radiate and others that evanesce.  The $x = 10.0 D_j$ line, for example, exhibits a similar, greater-than-$1/r^2$ rolloff at all three frequencies because the line is mostly outside the main radiation lobe and slices through a region where the directivity varies sharply. But, at 1.0 kHz, the only viable explanation for the steeper rolloff in the downstream locations is exponential amplitude decay due to the hydrodynamic field.  If the downstream, near-field intensity at 1.0 kHz in Fig. 5 were dominated by acoustic radiation that for some reason pointed directly along the shear layer, then the spreading would be expected to be nearly cylindrical.

13

American Institute of Aeronautics and Astronautics
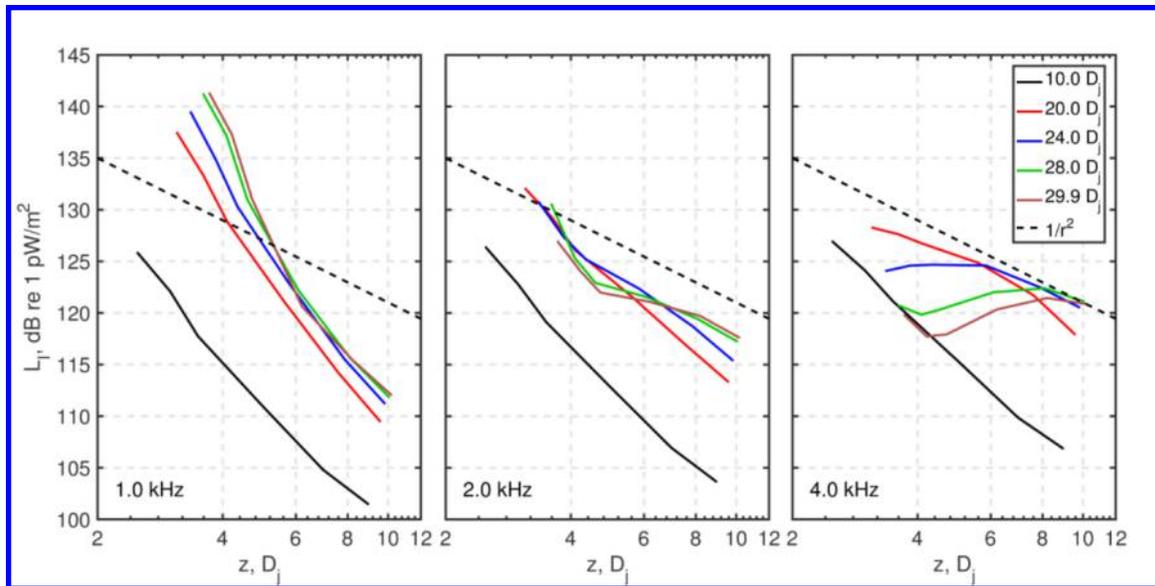
**Figure 8. Radial intensity decay as a function of sideline distance, z, at the probe locations for five downstream distances; see Fig. 1.**

The second observation regards the distance at which the hydrodynamic field is to be considered important. For example, Grizzi *et al.*'s analysis was conducted with microphones located 4 $D_j$ from the shear layer; Kuo *et al.*'s microphones ranged from $z = 2$ to 7 $D_j$ depending on downstream distance. This intensity analysis shows that the microphones between $z = 6.5$ to 8.4 $D_j$ are influenced by the hydrodynamic field below 3.0 kHz (St = 0.12) for this weakly convectively supersonic jet. As the convective Mach number is increased and the jet becomes a more efficient radiator due to enhanced Mach wave radiation, it is expected that the hydrodynamic field will play less of a role. In some sense, this has been already seen for small-scale solid rocket motor intensity measurements with the same propellent used in the Space Shuttle solid rocket boosters[20]. In that case, measurements were made only slightly more than 1 $D_j$ from the shear layer, and although the calculated intensity map demonstrated a downstream shift of the noise source region at low frequencies, there is no evidence of vectors pointed along the shear layer.

The final observation regards the somewhat remarkable interpretation of the hydrodynamic field as being an active intensity field that is measured using a multimicrophone intensity probe. Traditionally, the active intensity is described as the time-averaged product of the pressure and the in-phase portion of the particle velocity; the integral of its normal component over a surface provides calculated radiated power. The reactive intensity component, which is the product of the pressure and quadrature-phase portion of the particle velocity, typically describes the near-field non-radiating components. What makes the hydrodynamic field unique is that it is, in fact, a traveling disturbance, with a measurable time-averaged phase gradient, $\nabla\phi$, that results in an active intensity. It is a nonacoustic intensity in the sense that the pressure disturbance does not advect downstream at the ambient sound speed, but the PAGE method effectively sees a superposition of two active intensities – the hydrodynamic intensity and the radiated acoustic intensity.

As indicated previously, the active intensity is typically responsible for resulting in the radiated power. This begs an important question, however, one that cannot be fully answered by this study. In beam theory, subsonic flexural waves traveling along an *infinite* one-dimensional beam do not radiate. However, for a *finite* beam, there is radiation because of the portion of the wavenumber spectrum that is now supersonic. There are phenomenological analogies that can made with wavepackets[56] for subsonic jets and a mechanism for radiation, where it has also been shown that wavepacket jitter results in enhanced radiation. The question posed is this: Does this finite-length, subsonically advecting hydrodynamic field play any role in low-frequency, far-field radiation to shallow angles? Far downstream of the nozzle, beyond the end of the supersonic core, where low frequencies are generated, is there a blurring between the acoustic source and hydrodynamic disturbances? The answer to this question may be no, but perhaps it provides a clue as to the cause for the invariance in far-field directivity at very low frequencies (10 Hz), reported for the F-35B across all engine conditions from 25% engine thrust request through afterburner[57].

American Institute of Aeronautics and Astronautics

## VII.  Conclusion

In this paper, the phase and amplitude gradient estimator method[17] with phase unwrapping[18] has been applied to the calculation of vector acoustic intensity from multiple pressure microphone measurements has been applied to the aeroacoustic source characterization of a supersonic, laboratory-scale jet. The bandwidth of traditional intensity measurements for the same probe hardware has been increased by more than an order of magnitude, whereas prior measurements of full-scale rocket and military jet noise environments had suggested an upper frequency improvement of approximately three to five times. The analysis has resulted in a determination of the near-field energy flow, including the sharp transition between downstream Mach wave radiation and sideline radiation. Furthermore, the radiated intensity angles and approximate dominant source locations and their agreement with far-field directivity patterns and with other studies of jets with similar conditions has been established. Finally, some characteristics of the hydrodynamic near field have been explored, including the surprising finding that the hydrodynamic contribution to the near-field pressure field is a form of active intensity.  In sum, the analyses point to the utility of making vector intensity measurements of jet noise radiation, particularly as physical insights for the noise field from installed engines or due to jet impingement[58] are sought.

## Acknowledgments

## References

[1] Laufer, J., Schlinker, R. H., and Kaplan, R. E., "Experiments on Supersonic Jet Noise", *AIAA Journal,* Vol. 14, No. 4, April 1976, pp. 489-497.

[2] Papamoschou, D., "Imaging of Distributed Directional Noise Sources," AIAA paper 2008-2885, May 2008.

[3] Dougherty, R. P., "Improved generalized inverse beamforming for jet noise," *International Journal of Aeroacoustics*, Vol. 11, No. 3, 2012, pp. 259-290.

[4] Harker, B. M., Gee, K. L., Neilsen, T. B., Wall, A. T., and James, M. J., "Wavepacket Modeling and Full-scale Military Jet noise Beamforming Analyses, "AIAA paper 2016-2129, January 2016.

[5] Wall, A. T., Gee, K. L., Neilsen, T. B., McKinley, R. L., and James, M. M., "Military Jet Noise Source Imaging using Multisource Statistically Optimized Near-field Acoustical Holography," *Journal of the Acoustical Society of America,* Vol. 139, No. 4, 2016, pp. 1938-1950.

[6] Vold, H., Shah, P. N., Davis, J., Bremner, P. G., McLaughlin, D., Morris, P., Veltin, J., and McKinley, R., "High-resolution continuous scan acoustical holography applied to high-speed jet noise," AIAA paper 2010-3754, 2010.

[7] Wall, A. T., Gee, K. L., Neilsen, T. B., Krueger, D. W., and James, M. M., "Cylindrical acoustical holography applied to full-scale jet noise," *Journal of the Acoustical Society of America*, Vol. 136, 2014, pp.1120–1128.

[8] ISO 9614-1:1993, Acoustics—Determination of sound power levels of noise sources using sound intensity—Part 1: Measurement at discrete points (International Organization for Standardization, Geneva, Switzerland, 1993).

[9] ISO 9614-2:1996, Acoustics—Determination of sound power levels of noise sources using sound intensity—Part 2: Measurement by scanning (International Organization for Standardization, Geneva, Switzerland, 1996).

[10] ISO 9614-3:2002, Acoustics—Determination of sound power levels of noise sources using sound intensity—Part 3: Precision method for measurement by scanning (International Organization for Standardization, Geneva, Switzerland, 2002).

[11] Astrup, T., "Measurement of sound power using the acoustic intensity method –A consultant's viewpoint," *Applied Acoustics*, Vol 50, 1997, pp. 111–123.

[12] ISO 15186-2:2010, Acoustics—Measurement of sound insulation in buildings and of building elements using sound intensity—Part 1I: Field measurements (International Organization for Standardization, Geneva, Switzerland, 2003).

[13] Ventakesh, S. R., Poak, D. R., and Narayana, S., "Beamforming algorithm for distributed source localization and its application to jet noise," *AIAA Journal*, Vol. 41, 2003, pp. 1238–1246.

[14] Yu, C., Zhou, Z., and Zhuang, M., "An acoustic intensity-based method for reconstruction of radiated fields," *Journal of the Acoustical Society of America*, Vol. 123, 2008, pp. 1892–1901.

[15] Jaeger, S. M., and Allen, C. S., "Two-dimensional sound intensity analysis of jet noise," AIAA paper 1993-93-4342, 1993.

[16] Fisher, M. J., Harper-Bourne, M., and Glegg, S. A. L., "Jet Noise Source Location: The Polar Correlation Technique," *Journal of Sound and Vibration,* Vol. 51, 1977, pp. 23-54.

[17] Thomas, D. C., Christensen, B. Y., and Gee, K. L., "Phase and Amplitude Gradient Method for the Estimation of Acoustic Vector Quantities," *Journal of the Acoustical Society of America*, Vol. 137, 2015, pp. 3366-3376.

[18] Gee, K. L., Neilsen, T. B., Sommerfeldt, S. D., Akamine, M., and Okamoto, K., "Experimental validation of acoustic intensity bandwidth extension by phase unwrapping," *Journal of the Acoustical Society of America*, Vol. 141, 2017, pp. EL357–EL362.

[19] Gee, K. L., Giraud, J. H., Blotter, J. D., and Sommerfeldt, S. D., "Energy-based acoustical measurements of rocket noise," AIAA paper 2009-3165, 2009.

[20] Gee, K. L., Giraud, J. H., Blotter, J. D., and Sommerfeldt, S. D., "Near-field acoustic intensity measurements of a small solid rocket motor," *Journal of the Acoustical Society of America*, Vol. 128, 2010, pp. EL69-EL74.

[21] Gee, K. L., Whiting, E. B., Neilsen, T. B., James, M. M., and Salton, A. R., "Development of a near-field intensity measurement capability for static rocket firings," *Transactions of JSASS Aerospace Technology, Japan*, Vol. 14, 2016, No. ists30, pp. Po_2_9-Po_2_15.

[22] Stout, T. A., Gee, K. L., Neilsen, T. B., and Wall, A. T., "Acoustic intensity near a high-powered military jet aircraft," *Journal of the Acoustical Society of America*, Vol. 138, 2015, pp. EL1-EL7.

[23] Stout, T. A., Gee, K. L., Neilsen, T. B., Wall, A. T., and James, M. M., "Source characterization of full-scale jet noise using vector intensity," *Noise Control Engineering Journal,* Vol. 63, 2015, pp. 522-536.

[24] Fahy, F. J., "Measurement of acoustic intensity using the cross-spectral density of two microphone signals," *Journal of the Acoustical Society of America*, Vol. 62, 1977, pp. 1057-1059.

[25] Pavic, G., "Measurement of sound intensity," *Journal of Sound and Vibration,* Vol. 51, 1977, pp. 533–545.

[26] Pascal, J. C., and Li, J. F., "A systematic method to obtain 3D finite-difference formulations for acoustic intensity and other energy quantities," *Journal of Sound and Vibration,* Vol. 310, 2008, pp. 1093 – 1111.

[27] Wiederhold, C. P., Gee, K. L., Blotter, J. D., and Sommerfeldt, S. D., "Comparison of methods for processing acoustic intensity from orthogonal multimicrophone probes," *Journal of the Acoustical Society of America*, Vol. 131, 2012, pp. 2841-2852.

[28] Wiederhold, C. P., Gee, K. L., Blotter, J. D., Sommerfeldt, S. D., and Giraud, J. H., "Comparison of multimicrophone probe design and processing methods in measuring acoustic intensity," *Journal of the Acoustical Society of America*, Vol. 135, 2014, pp. 2797-2807.

[29] Mann, J. A. III, Tichy, J., and Romano, A. J., "Instantaneous and time-averaged energy transfer in acoustic fields," *Journal of the Acoustical Society of America*, Vol. 82, 1987, pp. 17–30.

[30] Mann, J. A. III, and Tichy, J., "Acoustic intensity analysis: Distinguishing energy propagation and wave-front propagation," *Journal of the Acoustical Society of America*, Vol. 90, 1991, pp. 20–25.

[31] Mann, J. A. III, and Tichy, J., "Near-field identification of vibration sources, resonant cavities, and diffraction using acoustic intensity measurements," *Journal of the Acoustical Society of America*, Vol. 90, 1991, pp. 720–729.

[32] Greska, B., "Supersonic jet noise and its reduction using microjet injection," Ph.D. thesis, The Florida State University, FAMU-FSU Collage of Engineering, 2005.

[33] Akamine, M., Nakanishi, Y., Okamoto, K., Teramoto, S., Okunuki, T., and Tsutsumi, S, "Acoustic phenomena from correctly expanded supersonic jet impinging on inclined plate," *AIAA Journal*, Vol. 53, pp. 2061-2067.

[34] Oertel, H., and Patz, G., "Wirkung von unterschallmanteln auf die Machwellen in der umgebung von Uberschallstrahlen," *ISL Report RT 505/81*. Institut Franco-Allemand De Recherches, Saint-Louis, France.

[35] Baars, W. J., Tinney, C. E., Murray, N. E., Jansen, B. J., and Panickar, P., "The effect of heat on turbulent mixing noise in supersonic jets," AIAA paper 2011-1029, 2011.

[36] Baars, W. J., "Acoustics from high-speed jets with crackle," Ph.D. Dissertation, University of Texas at Austin (2013).

[37] Panda, J. & Seasholtz, R. G., "Experimental investigation of density fluctuations in high-speed jets and correlation with generated noise," *Journal of Fluid Mechanics*, Vol. 450, 2002, pp. 97–130.

[38] Nagamatsu, H. T., and Horvay, G., "Supersonic jet noise," AIAA paper 1970-237, 1970.

[39] Witze, P. O., "Centerline velocity decay of compressible free jets," *AIAA Journal*, Vol. 12(4), 1794, pp. 417–4187.

[40] Bridges, J., and Wernet, M., "Measurement of the Aeroacoustic Sound Source in Hot Jets," AIAA paper 2003-3130, May 2003.

[41] Viswanathan, K., "Investigation of the Sources of Jet Noise," AIAA paper 2007-3601, 2007.

[42] Panda, J., Seasholtz, and Elam, K. A., "Investigation of Noise Sources in High-speed Jets via Correlation Measurements," *Journal of Fluid Mechanics,* Vol. 537, 2005, pp. 349-385.

[43] Lee, S. S. and Bridges, J., "Phased-array Measurements of Single-flow Hot Jets," AIAA paper 2005-2842, 2002.

[44] James, M. M., Salton, A. R., Gee, K. L., Neilsen, T. B., McInerny, S. A., and Kenny, R. J., "Modification of Directivity Curves for a Rocket Noise Model," *Proceedings of Meetings on Acoustics,* Vol. 18, 2014, paper 040008.

[45] Baars, W. J., Tinney, C. E., Wochner, M. S., and Hamilton, M. F., "On Cumulative Nonlinear Acoustic Waveform Distortions from High-speed Jets," *Journal of Fluid Mechanics,* Vol. 749, 2014, pp. 331-366.

[46] Tam, C. K. W., Viswanathan, K., Ahuja, K. K., and Panda, J., "The sources of jet noise: Experimental evidence," *Journal of Fluid Mechanics*, Vol. 615, 2008, pp. 253-292.

[47] Vaughn, A. B., Neilsen, T. B., Gee, K. L., Okamoto, K., and Akamine, M., "Near-field spatial variation in similarity spectra decomposition of a Mach 1.8 laboratory-scale jet," *Proceedings of Meetings on Acoustics*, Vol. 29, 2017, paper in press.

[48] Neilsen, T. B., Vaughn, A. B., Gee, K. L., Akamine, M., Okamoto, K. Teramoto, S., and Tsutsumi, S., "Level-educed Wavepacket Representation of Mach 1.8 Laboratory-Scale Jet Noise," Submitted to 2017 *AIAA Aeroacoustics Conference*, AIAA paper 2017-xxxx.

[49] Torrie, D. K., Whiting, E. B., Gee, K. L., Neilsen, E. B., and Sommerfeldt, S. D., "Initial laboratory experiments to validate a phase and amplitude gradient estimator method for the calculation of acoustic intensity," *Proceedings of Meetings on Acoustics*, Vol. 23, 2015, paper 030005.

16

American Institute of Aeronautics and Astronautics

[50] Whiting, E. B., "Energy Quantity Estimation in Radiated Acoustic Fields," M.S. Thesis, Brigham Young University, Provo, UT, 2016.

[51] Akamine, M., Okamoto, K., Gee, K. L., Neilsen, T. B., Teramoto, S., Tsutsumi, S., Okunuki, T., "Comparison of acoustic intensity vectors with SPL and phase distributions of supersonic jet," *8th Asian Joint Conference on Propulsion and Power*, March 2016.

[52] Tam, C. K. W., "Supersonic jet noise," *Annual Review of Fluid Mechanics*, Vol. 27, 1995, pp. 27–43.

[53] Papamoschou, D., Morris, P. J., and McLaughlin, D. K., "Beamformed Flow-Acoustic Correlations in High-Speed Jets," AIAA paper 2009-3212, May 2009.

[54] Grizzi, S., Casmussi, R., and DiMarco, A., "Experimental Investigation of pressure fluctuations in the near field of subsonic jets at different Mach and Reynolds numbers," AIAA paper 2012-2257, June 2012.

[55] Kuo, C.-W., Buisson, Q., McLaughlin, D. K., and Morris, P. J., "Experimental Investigation of Near-field Pressure Fluctuations Generated by Supersonic Jets," AIAA paper 2013-2033, May 2013.

[56] Jordan, P., and Colonius, T., "Wave packets and turbulent jet noise," *Annual Review of Fluid Mechanics,* Vol. 45, 2013, pp. 173–195.

[57] James, M. M., Salton, A. R., Downing, J. M., Gee, K. L., Neilsen, T. B., Reichman, B. O., McKinley, R., Wall, A. T., and Gallagher, H. "Acoustic Emissions from F-35 Aircraft during Ground Run-Up," AIAA paper 2015-2375, June 2015.

[58] Akamine, M., Okamoto, K., Gee, K. L., Neilsen, T. B., Teramoto, S., Okunuki, T., and Tsutsumi, S., "Effect of Nozzle-Plate Distance on Acoustic Phenomena from Supersonic Impinging Jet," AIAA paper 2016-2930, June 2016.

American Institute of Aeronautics and Astronautics